Available online at www.sciencedirect.com
SCIENCE DIRECT®
DNA Repair 3 (2004) 1601–1615
DNA REPAIR
www.elsevier.com/locate/dnarepair

Cell cycle regulation of the murine 8-oxoguanine DNA glycosylase (mOGG1): mOGG1 associates with microtubules during interphase and mitosis

Kimberly A. Conlon[a], Dmitry O. Zharkov[b], Miguel Berrios[a,c,*]

[a] *Department of Pharmacological Sciences, School of Medicine, University Hospital and Medical Center, State University of New York, 100 Nicholls Road, Stony Brook, New York 11794-8651, USA*
[b] *Novosibirsk Institute of Chemical Biology and Fundamental Medicine, 8 Lavrentieva Avenue Novosibirsk 630090, Russia*
[c] *University Microscopy Imaging Center, State University of New York, Stony Brook, New York 11794-8088, USA*

Received 3 March 2004; received in revised form 14 June 2004; accepted 15 June 2004
Available online 14 July 2004

Abstract

8-Oxoguanine DNA glycosylase (OGG1) is a major DNA repair enzyme in mammalian cells. OGG1 participates in the repair of 8-oxoG, the most abundant known DNA lesion induced by endogenous reactive oxygen species in aerobic organisms. In this study, antibodies directed against purified recombinant human OGG1 (hOGG1) or murine (mOGG1) protein were chemically conjugated to either the photosensitizer Rose Bengal or the fluorescent dye Texas red. These dye–protein conjugates, in combination with binding assays, were used to identify associations between mOGG1 and the cytoskeleton of NIH3T3 fibroblasts. Results from these binding studies showed that mOGG1 associates with the cytoskeleton by specifically binding to the centriole and microtubules radiating from the centrosome at interphase and the spindle assembly at mitosis. Similar results were obtained with hOGG1. Together results reported in this study suggest that OGG1 is a microtubule-associated protein itself or that OGG1 utilizes yet to be identified motor proteins to ride on microtubules as tracks facilitating the movement and redistribution of cytoplasmic OGG1 pools during interphase and mitosis and in response to oxidative DNA damage.

Keywords: Cell cycle; DNA repair; Fibroblasts; MAPs; Microtubules; Mitosis; OGG1

1. Introduction

Endogenous reactive oxygen species (ROS) are byproducts from aerobic metabolism. ROS formation in vivo increases when cells are exposed to environmental pollutants [1,2], certain drugs [3], nutrient deprivation [4], oxidizing agents or ionizing radiation [5–7] and during some pathological processes such as inflamation or ischemia-reperfusion [8]. Reaction between ROS and DNA leads to modifications of several types, including single or double strand breaks, as well as modifications of bases and sugars. Damage to genomic DNA often results in mutations that may lead to neoplasia, cell death and degenerative diseases [9–12]. Although cellular anti-oxidant defenses (e.g., catalase, peroxidase, superoxide dismutase) can effectively combat the effects of ROS, those that escape these defenses can diffuse into the nucleus to react with DNA [13].

ROS generate several base modifications in DNA including 7,8-dihydro-8-oxoguanine (8-oxoG). 8-OxoG is a relatively stable oxidized form of guanine frequently produced by ROS when interacting with either free nucleotides or DNA [14]. At replication, 8-oxoG will often be mispaired with adenine, giving rise to G:C to T:A transversions, a common somatic mutation associated with human cancers. 8-OxoG has also been shown to be miscoding in vitro and mutagenic in vivo [15]. As a result, 8-oxoG has been used as a marker for oxidative DNA damage [13,16].

* Corresponding author. Tel.: +1 631 444 3050; fax: +1 631 444 3218.
E-mail address: miguel@pharm.sunysb.edu (M. Berrios).

1568-7864/$ – see front matter © 2004 Elsevier B.V. All rights reserved.
doi:10.1016/j.dnarep.2004.06.011

8-OxoG-DNA repair activities have been reported in mammals including mice [17,18], human leukocytes and HeLa cells [19,20]. The murine OGG1 (*mOGG1*) gene was localized to chromosome 6 [21], and the gene product was identified as a DNA 8-oxoG glycosylase [18]. The human OGG1 gene has been localized to the short arm of chromosome 3 (3p25/26) in a region that is commonly deleted in lung cancers [22]. Recently, liver cells from homozygous $ogg^{-/-}$ mice have shown a 10-fold increase in G:C to T:A transversion frequencies in their DNA [23,24].

Human OGG1 gene generates several isoforms by alternative splicing; all isoforms have been localized to mitochondria except for one containing a single NLS that has been localized to the nucleus [25–28]. Similarly, antibodies directed against hOGG1 or hMYH, the human homolog for MutY, another DNA glycosylase directed against oxidative DNA damage, localized these enzymes to mitochondria and nuclei of human cells, and their distribution was regulated by alternative splicing of each transcript [29,30]. Furthermore, using transiently expressed epitope-tagged human OGG1, hMYH and the human homolog of yet another repair enzyme edonuclease III (hNTH1), Takao and collaborators showed that these enzymes were localized mostly to the nucleus and mitochondria in transfected Cos7 cells [26]. Recently, using a stable transfectant cell line expressing human OGG1 fused at the C-terminus to GFP, it was shown that human OGG1 was preferentially associated with a nuclear matrix or karyoskeleton-enriched fraction and chromatin during interphase and becomes associated with mitotic chromosomes during mitosis [31]. It is now accepted that there are distinct nuclear and cytoplasmic pools of OGG1, with the former composed of a single isoform, OGG1-1a, and the latter, of several isoforms lacking the nuclear localization signal [26,27]. Activity, expression and subcellular distribution of OGG1 is modulated by a number of circumstances causing oxidative DNA damage [1–8].

We previously reported that cytoplasmic pools of mOGG1 redistribute to the nucleus and nuclear periphery in response to nutrient deprivation and oxidative DNA damage [4]. The relatively rapid redistribution of mOGG1 observed in cells exposed to oxidative stress suggested that the movement of intracellular mOGG1 pools may be mediated, in part, by active transport rather than just diffusion through the cytosol. This recent observation together with a previous report showing the association of OGG1 with the nuclear matrix or karyoskeleton [31] suggests that relationships similar to those observed in the nucleus may also exist between OGG1 and elements of the cytoskeleton of eukaryotic cells. The cytoskeleton is a filamentous network spanning the cytoplasm and composed of three major cytoskeletal polymers: actin filaments, intermediate filaments and microtubules. These filaments interact with each other and with many different associated proteins to mediate the trafficking of macromolecules and small organelles through the cytoplasm [32–36]. The apparent universality of this bidirectional trafficking is substantiated by the wide range of macromolecules transported by cytoskeletal filaments, including ribosomal components, other ribonucleoproteins, cytosolic proteins, etc. For example, cells use the cytoskeleton to regulate the trafficking of mRNAs and cofactors from transcription and processing sites in the nucleus to translation and degradation sites in the cytosol [37,38].

Microtubules are hollow cylindrical structures approximately 25 nm in diameter and can reach 25 μm in length. Each is constructed of 13 protofilaments formed by tubulin molecules, relatively stable heterodimers of alpha and beta tubulin subunits. Besides serving other functions, microtubules, in conjunction with microtubule-associated proteins (MAPs) and molecular motor proteins, provide paths along which macromolecules (i.e. mRNAs and proteins) are transported to or from the nucleus or elsewhere in the cytosol [39,40]. Association with microtubules facilitates not only the distribution of specific macromolecules to a targeted cell region but also prevents these macromolecules from being diluted in the cytosol [38]. Microtubules also form the centrioles at the core of centrosomes (see, e.g., [41]). In addition to participating in the organization of microtubules and the mitotic spindle assembly, centrosomes have been shown to play a critical role in cell cycle progression and cellular responses to DNA replication defects and DNA damage [42,43].

Although most studies have been focused on elucidating the expression, enzyme mechanism and substrate specificity of the mammalian OGG1 protein, the role that cytoskeletal components may play in regulating the distribution of OGG1 pools within cells has not yet been evaluated. This study used several strategies to circumvent limitations associated with the use of actively growing tissue culture cells not over expressing OGG1 including the combination of binding assays, chemical cross-linking and in situ site-directed photochemistry to establish whether OGG1 associates with elements of the cytoskeleton as an effective pathway to regulate its redistribution in normally growing cells as well as in response to oxidative stress and DNA damage. Results from this study showed that OGG1 specifically binds to microtubules in actively growing cells. OGG1 remained largely bound to a network of microtubules and the mitotic spindle assembly during interphase and mitosis respectively suggesting that OGG1, and other DNA repair proteins, may bind to microtubules and/or use MAPs or molecular motors riding on microtubules to relocate repair enzyme pools in cells growing under normal and oxidative stress conditions and during the cell cycle.

2. Materials and methods

2.1. Materials

Bovine serum albumin (BSA), Coomassie blue, cyanogen bromide activated agarose beads, dithiothreitol (DTT), formamide, ethylenediaminetetraacetic acid (EDTA), FITC-conjugated phalloidin (from *A. phalloides*), iodoacetamide (IAA), isopropyl beta-D-thiogalactopyranoside (IPTG) were

purchased from Sigma Chemical Co. (St. Louis, MO). Mammalian tubulin (from bovine brain) was purchased from Cytoskeleton Inc. (Denver, CO). Paraformaldehyde, Triton X-100 and trichloroacetic acid (TCA) were purchased from Fisher Scientific Co. (Springfield, NJ). Sodium dodecyl sulfate (SDS) was purchased from British Drug Houses (Poole, England). Dimethyl suberimidate (DMS) was purchased from Pierce (Rockford, IL). Bovine calf serum was purchased from HyClone (Logan, UT). Dulbecco's modified Eagle's medium (DMEM), penicillin G, streptomycin and L-glutamine were purchased from Invitrogen (Grand Island, NY). Acrylamide, *N*,*N*'methylene-bisacrylamide and *N*,*N*,*N*′,*N*′-tetramethylethylenediamine were purchased from Eastman Kodak Co. (Rochester, NY). CNBr-activated Sepahrose 4B, Sepharose MonoS HR 5/5, Q Sepharose, S Sepharose, Superdex 75HR 10/30 were purchased from Pharmacia (Uppsala, Sweden). Bccmount was purchased from BCC Microimaging (Stony Brook, NY). Vector pET-15b DNA and *E. coli* BL21(DE3) cells were from Novagen (Madison, WI). Restriction endonuclease *Xho*I and T4 DNA ligase were purchased from New England Biolabs (Beverly, MA). Restriction endonuclease *Bpu*1102I and *Pfu* DNA polymerase were from Stratagene (La Jolla, CA). All other chemicals were obtained commercially, were of reagent grade, and were used without further purification.

2.2. Antibodies

Rabbit anti-mOGG1 antiserum directed against the whole wild-type recombinant mOGG1 polypeptide was essentially as previously described [44]. Rabbit anti-bovine brain tubulin antibodies were provided by BCC Microimaging (Stony Brook, NY). FITC-conjugated mouse monoclonal anti-tubulin was purchased from Sigma Chemical Co. (St. Louis, MO). Mouse monoclonal antibody mAb1636 with reactivity against desmin, an intermediate filament protein was purchased from Chemicon International (Temecula, CA). Affinity purified goat anti-rabbit IgG (H&L chains) conjugated to Alexa 488 and affinity purified goat anti-mouse IgG (H&L chains) conjugated to Alexa 568 were purchased from Molecular Probes (Eugene, OR).

2.3. Expression and purification of human and mouse OGG1

Expression and purification of wild-type recombinant mOGG1 was as previously described [44]. Cloning and overexpression of hexahistidine-tagged human OGG1 (isoform 1a) will be described elsewhere (D.O.Z., manuscript in preparation).

2.4. Conjugation of the N-hydroxysuccinimide ester of Rose Bengal hexanoic acid (RBHA-NHS) to anti-mOGG1 antibodies

Chemical conjugation of RBHA-NHS to rabbit anti-mOGG1 antibodies was conducted as previously described [45]. Briefly, to 200 μl of an ice cold solution containing rabbit anti-mOGG1 antibodies was added 40 μg of RBHA-NHS in DMSO. The mixture was incubated at room temperature for 1 h on a Roto-Shake Genie (Scientific Industries, Bohemia, NY). Conjugate mixtures were dialyzed against 200 ml of 20% (v/v) glycerol in 140 mM sodium chloride; 10 mM phosphate buffer, pH 7.4 (PBS) at 4 °C overnight. Antibody conjugates were stored at −20 °C until use.

2.5. Conjugation of recombinant mOGG1 and hOGG1 to the N-hydroxysuccinimide (NHS) esters of Texas red, Alexa series dyes and Rose Bengal hexanoic acid

Chemical conjugation of mOGG1 and hOGG1 to the NHS esters of Texas red, Alexa series dyes and Rose Bengal hexanoic acid was as follows: to 100 μl containing purified recombinant mOGG1 (1.6 mg/ml) or hOGG1 (0.75 mg/ml) was added 1 μl of 20% (w/v) SDS, followed by either 1 μg of Texas Red-NHS, 2 μg of $Alexa_{488}$-NHS, 1 μg of $Alexa_{568}$-NHS, or 1 μg of RBHA-NHS in DMSO. Reaction mixtures were incubated for 30 min at room temperature on a Roto-Shake Genie (Scientific Industries, Bohemia, NY). After incubation, reaction mixtures were dialyzed against 20 ml of 20% (v/v) DMSO in 10 mM phosphate buffer, pH 7.4. Dye conjugates were stored at 4 °C until use.

2.6. Tissue culture

NIH3T3 fibroblasts were obtained from the American Type Culture Collection (Manassas, VA) and kept frozen in liquid nitrogen until use. Before use, NIH3T3 fibroblasts were thawed and cultured in DMEM supplemented with 10% (v/v) calf serum, 2 mM L-glutamine, 0.1 mM non-essential amino acids, 1 mM sodium pyruvate and 100 IU/ml penicillin G, 100 (g/ml streptomycin. Unless specified otherwise NIH3T3 fibroblasts were plated onto glass microscope slides in 10 cm tissue culture dishes at a density of 2–5 × 10^5 cells/dish for mOGG1 binding studies, in situ photochemistry and indirect immunofluorescence staining [45]. To enrich for cells in mitosis, cells growing on microscope slides and culture media containing free (floater) cells were mounted onto a Cytobucket (IEC, Needham Heights, MA) customized to fit two-well immunofluorescent chambers (EMS, Port Washington, PA) and centrifuged at 400 × *g* for 40 min in a Centra-CL3 Series centrifuge (Thermo IEC, Needham Heights, MA). After centrifugation, the media was removed and cells fixed with paraformaldehyde essentially as described for immunofluorescence microscopy.

2.7. In situ photochemistry

In situ photochemistry was performed essentially as previously described [45]. Briefly, NIH3T3 fibroblasts were grown on heat-sterilized but otherwise untreated glass microscope slides at a concentration of 45 cells/mm^2 as previously described [45]. Incubation with Rose Bengal-conjugated

mOGG1 (RB–mOGG1) or Rose Bengal-conjugated hOGG1 (RB–hOGG1) and irradiation with visible light were conducted in two-well immunofluorescence chambers (EMS, Fort Washington, PA) as follows: slides were mounted into immunofluorescence chambers and cells washed free of culture media with fresh MSM-Pipes. MSM-Pipes contained 18 mM $MgSO_4$; 5 mM $CaCl_2$; 41 mM KCl; 24 mM NaCl; 0.5% (v/v) Triton X-100; 0.5% (v/v) of either Tween 20 or Nonidet P40; 5 mM Pipes, pH 7.5 [46]. To each well, 200 μl of either RB–mOGG1 or RB–hOGG1 diluted 1:200 in MSM-Pipes were added. Control wells received either 200 μl of unconjugated mOGG1 or unconjugated hOGG1 diluted 1:200 in MSM-Pipes. Mixtures containing RB–OGG1 or unconjugated OGG1 were incubated in the dark for 30 min at 37 °C using a humidified chamber. After incubation, cells were washed three times with 400 μl of MSM-Pipes. After washings, 800 μl of MSM-Pipes were added, and cells were irradiated for 60 min at 37 °C with visible light from illumination heads connected through a 30 cm long, 5-mm diameter fiber optic to a fan-cooled 150 W halogen lamp (model 8375, Schott-Fostec, Auburn, NY). Each illumination head focused the light on the cells and reaction mixtures from a distance of 40 mm. The light intensity falling on each incubation mixture (immunofluorescence chamber well) was 2.2×10^4 Lux. Light intensity readings were made using a type 214 light meter (General Electric, Cleveland, OH).

2.8. In vitro photochemistry

In vitro photolysis of tubulin was essentially as previously described [47]. Briefly, solutions 10 μl containing 5 μg of bovine brain tubulin in MSM-Pipes were placed into clear borosilicate glass tubes. To each solution, 320 ng of RB–mOGG1 or 320 ng of unconjugated mOGG1 was added. Control mixtures were incubated in the dark at 37 °C for 15 min. Irradiation conditions were as previously described [47]. After irradiation, digestion products were characterized by SDS-PAGE.

2.9. Staining of filamentous actin (f-actin) with FITC-conjugated phalloidin

Fluorescent staining with FITC-conjugated phalloidin was performed using two-well immunofluorescence chambers as previously described [45]. Procedures were conducted at 37 °C. Briefly, cells were fixed with paraformaldehyde, washed with MSM-Pipes and incubated for 30 min at 37 °C with a freshly prepared solution containing 100 ng/ml FITC-conjugated phalloidin. After incubation, cells were rinsed once with MSM-Pipes. A glass coverslip was mounted over each sample with 4 μl of Bccmount.

2.10. Decoration of microtubules by fluorescently-tagged mOGG1

Decoration of network and mitotic assembly microtubules with Texas red-conjugated mOGG1 was performed using two-well immunofluorescence chambers. Procedures were conducted at room temperature unless specified. Briefly, cells were fixed with paraformaldehyde, washed with MSM-Pipes and incubated for 30 min at 37 °C with a freshly prepared 200 μl solution containing 600 ng Texas red-conjugated mOGG1. After incubation, cells were rinsed three times with MSM-Pipes, mounted with glass coverslips using 4 μl of Bccmount. Competition experiments were conducted as follows: 200 μl MSM-Pipes solutions containing either 600 ng Texas red-conjugated mOGG1 or a mixture of 600 ng Texas red-conjugated mOGG1 and 5 μg tubulin ("competitor") were pre-incubated for 15 min at 37 °C before probing cells. After pre-incubation, cells were fixed with paraformaldehyde, washed with MSM-Pipes and incubated for 15 min at 37 °C with either the solution containing 600 ng Texas red-conjugated mOGG1 or the solution containing a mixture of 600 ng Texas red-conjugated mOGG1 and 5 μg tubulin. After incubation, cells were rinsed three times with MSM-Pipes and mounted with glass coverslips as above.

2.11. Chemical cross-linking of mOGG1–tubulin complexes

Chemical cross-linking of proteins was performed as previously described [48]. Briefly, DMS chemical cross-linking experiments used cell homogenates and detergent-permeabilized cells. After cross-linking with DMS for 15 min, samples were diluted with buffer containing 2% (w/v) SDS and 62.5 mM Tris–HCl pH 6.8, and incubated for 10–20 min at room temperature to quench unreacted cross-linker. Samples were then boiled, cooled, and proteins were precipitated by addition of trichloroacetic acid to a final concentration of 10% (w/v). Resolubilized proteins were subjected to SDS-PAGE [49] and immunoblot analyses. Specific DMS concentration and conditions used were as indicated in the corresponding figure legend.

2.12. Affinity binding of mOGG1–tubulin complexes

Chemical conjugation of protein mixtures containing 100 μg mOGG1 plus 100 μg BSA or 200 μg BSA (control) to cyanogen bromide-activated Sepharose beads was performed according to the manufacturer's instructions. Affinity purification of tubulin using Sepharose-immobilized recombinant mOGG1 and BSA or Sepharose-immobilized BSA was as follows: Briefly, fractions enriched in bovine brain tubulin were incubated for 30 min at 37 °C with either 40 μl mOGG1/BSA-Sepharose beads or BSA-Sepharose beads in MSM-Pipes without detergents. After incubation, beads were washed as for immunoprecipitation [50], three times 5 min each in MSM-Pipes with detergents followed by two final washes with MSM-Pipes without detergents. After washings, beads were resuspended in SDS-PAGE loading buffer and proteins analyzed by SDS-PAGE.

2.13. SDS-PAGE

SDS-PAGE was as previously described [47]. Briefly, proteins were precipitated with 12% (w/v) TCA on ice for 15 min before centrifugation at 10,000 × *g* for 30 min. Supernatants were discarded and the resulting pellets were centrifuged at 10,000 × *g* for an additional 10 min, followed by careful removal of residual supernatants. Pellets were neutralized with 2 M Tris base, solubilized in sample loading buffer (2% (w/v) SDS; 10% (v/v) glycerol; 20 mM DTT; 62.5 mM Tris–HCl pH 6.8; 2 μg/ml bromophenol blue) and boiled for 5 min. Alkylation of thiol groups on proteins was performed by incubating supernatants in the presence of 20 mM IAA for 30 min at room temperature in the dark. SDS-PAGE gel-separated proteins were visualized using Coomassie blue. Gels were stained overnight.

2.14. Immunofluorescence

Cell fixation with paraformaldehyde and indirect immunofluorescence was as previously described [46]. After incubation with antibodies, cells were mounted under a glass coverslip with 4 μl of Bccmount.

2.15. Light microscopy

Specimens were examined with a Zeiss Axiophot epifluorescent photomicroscope (Carl Zeiss, Jena, Germany) using a Zeiss 40X/.75 planachromat phase objective lens. Wide-field micrographs were acquired using MaxIm DL/CCD image acquisition and processing software package (Diffraction Ltd., Ottawa, Canada) with a KX14E (A3156) cooled CCD camera system (Apogee Instruments, Auburn, CA) attached to the video port of the above microscope.

3. Results

3.1. Fluorescently-tagged mOGG1 decorates a network of microtubules at interphase and the mitotic spindle assembly at mitosis

We previously showed using specific antibodies in conjunction with indirect immunofluorescence microscopy that mOGG1 was largely localized to the cytoplasm of mammalian cells in culture and that the onset of oxidative DNA damage induced the redistribution of OGG1 pools from the cytoplasm to the nucleus and its peripheral cytoplasm [44]. These immunofluorescent localization studies also showed that, in some cells, it was possible to discern that cytoplasmic anti-mOGG1 antibody staining seemed not diffused throughout but associated with small mitochondrial-size bodies and organized along strands or filaments. The filamentous aspect of anti-mOGG1 antibody staining was puzzling since a similar staining pattern was observed when these cells had been probed with anti-8-oxoguanine antibodies [44].

To investigate further mOGG1 cytoplasmic distribution and substantiate previous observations, we probed cells with purified wild-type recombinant mOGG1 tagged with the fluorescent dye Texas red instead of using indirect immunofluorescence and anti-mOGG1 antibodies. If mOGG1 was associated with filamentous structures in the cytoplasm, then fluorescently-tagged mOGG1 may be a suitable probe to determine whether mOGG1 itself associates with elements of the cell cytoskeleton. MOGG1 was expressed in *E. coli*, purified and chemically conjugated to Texas red as described in Section 2. Results from these in situ localization experiments are shown in Fig. 1. When cells were fixed onto microscope slides, probed with TR–mOGG1 and examined under the epifluorescent microscope as described in Section 2, an extensive network of filaments spanning most of the cytoplasm was shown (Fig. 1B and D). TR–mOGG1-decorated filaments that were more densely packed near the periphery of the nucleus (Fig. 1B and D). Although these filaments spanned most of the cell, they seemed to exclude the outer most fringes of the cytoplasm (Fig. 1C and D (arrows)). Similar results to those shown in Fig. 1B and D were obtained when cells were probed with untagged mOGG1 instead and stained for indirect immunofluorescence microscopy with anti-mOGG1 antibodies (not shown). No filamentous network was detected when cells were probed with fluorescently-tagged BSA (not shown). Thus, chemical conjugation to Texas red did not confer mOGG1 its affinity for cytoplasmic filaments.

To ascertain the nature of the filamentous network decorated by mOGG1 and whether it corresponded to any of the three major protein polymers of the cytoskeleton: actin filaments, intermediate filaments or microtubules, cells were probed with TR–mOGG1 and either FITC-tagged phalloidin, anti-desmin antibodies or FITC-tagged anti-α tubulin antibodies. Cell staining with FITC-tagged phalloidin and immunofluorescence with anti-desmin antibodies or anti-tubulin antibodies was as described in Section 2. Results from these in situ localization analyses are shown in Fig. 2. Cells probed with FITC-tagged phalloidin, a toxin that specifically binds to filamentous actin (f-actin) [51,52], showed a staining pattern that was consistent with f-actin and actin stress fibers (Fig. 2B). The fluorescent staining pattern shown by fluorescently-tagged phalloidin was distinct from the filaments decorated by TR–mOGG1 (Fig. 2A). Similarly, cells probed with antibodies directed against desmin, a class III intermediate filament protein [53,54], showed a staining pattern which was consistent with intermediate filament distribution (Fig. 2D) but different from the filamentous network decorated by TR–mOGG1 (Fig. 2C). Cells probed with antibodies directed against tubulin, however, showed a staining pattern (Fig. 2F) that was similar to that shown by TR–mOGG1 probed cells (Fig. 2E). Furthermore, microtubule staining with TR–mOGG1 was eliminated under conditions that depolymerized microtubules (e.g., cold) (not shown).

To explore the possibility that TR–mOGG1 may also associate with microtubules organizing the mitotic spindle assembly, cells at various stages of mitosis were fixed and

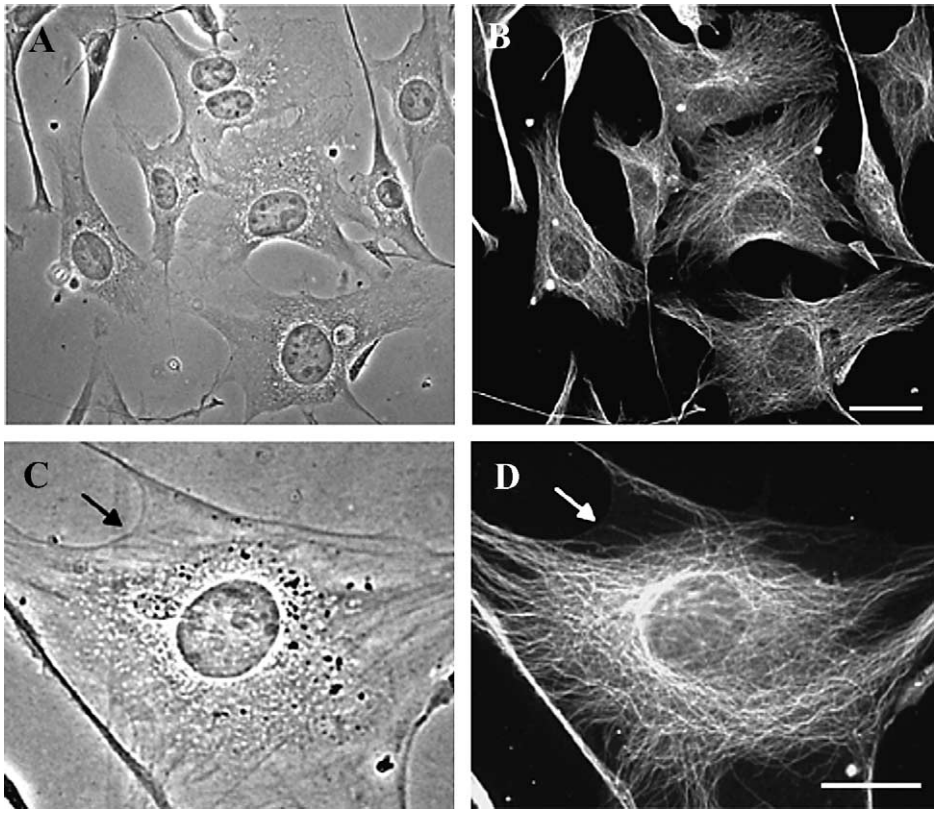

Fig. 1. Staining of NIH-3T3 fibroblasts with fluorescently-tagged recombinant mOGG1. Chemical conjugation of recombinant mOGG1 to Texas red and cell probing with TR–mOGG1 was as described in Section 2. (A, C) Phase contrast micrographs. (B, D) Epifluorescent micrographs. (A–D) NIH3T3 fibroblasts probed with TR–mOGG1. (C, D) membrane ruffles (arrows). (B) Bar, 25 μm. (D) Bar, 20 μm.

probed with TR–mOGG1. Cells at different stages of mitosis were collected from otherwise untreated actively growing cultures by low-speed centrifugation, fixed onto slides and probed with TR–mOGG1 as described in Section 2. Results from these experiments are shown in Fig. 3. When actively dividing cells were probed with TR–mOGG1 and examined by epifluorescent microscopy, images revealed that TR–mOGG1 was capable of decorating the mitotic spindle assembly (Fig. 3). TR–mOGG1 decorated interpolar (Fig. 3A–D) as well as astral microtubules emanating from the spindle poles (Fig. 3D (arrow)). The spindle poles were identified using anti-γ tubulin antibodies (not shown). TR–mOGG1 also showed diffused staining throughout these dividing cells (Fig. 3). This diffuse staining excluded the space occupied by the highly condensed mitotic chromosomes, however (Fig. 3A (arrows)). The space occupied by mitotic chromosomes was identified using specific dyes for DNA (not shown). TR–mOGG1 decorated mitotic cells in a manner similar to that shown by anti-tubulin antibodies using immunofluorescence (not shown).

3.2. TR–mOGG1 decorates the centriole at the core of the centrosome of interphase cells

To evaluate the extent and specificity by which TR–mOGG1 decorates tubulin polymeric structures in mammalian cells, TR–mOGG1 decoration of the centriole was also assessed by epifluorescent microscopy. Results from these experiments are shown in Fig. 4. Centrioles were identified using specific antibodies for γ tubulin (Fig. 4B (arrows)). Epifluorescent microscopy showed that TR–mOGG1 also decorates the centriole in interphase cells (Fig. 4C–E (arrows)). Centriole staining by TR–mOGG1 was similar to that obtained with anti-tubulin antibodies and immunofluorescence microscopy (not shown).

Similar results to those shown in Figs. 1–4 were obtained when fluorescent dyes from the Alexa series were conjugated to mOGG1 or Texas red was chemically conjugated to hexahistidine-tagged recombinant hOGG1 (TR–hOGG1) and used to probe NIH3T3 fibroblasts (not shown). Chemical conjugation of mOGG1 to Alexa series dyes and cell probing with Alexa series-mOGG1 conjugates was as described in Section 2. Expression and purification of recombinant hOGG1, chemical conjugation to Texas red and cell probing with TR–hOGG1 conjugates was as described for TR–mOGG1 or as described in Section 2.

3.3. Protein fractions enriched in mammalian tubulin inhibit the decoration of microtubules by TR–mOGG1 in situ

Although in our hands the decoration of microtubules, the centriole and the mitotic spindle assembly by TR–mOGG1

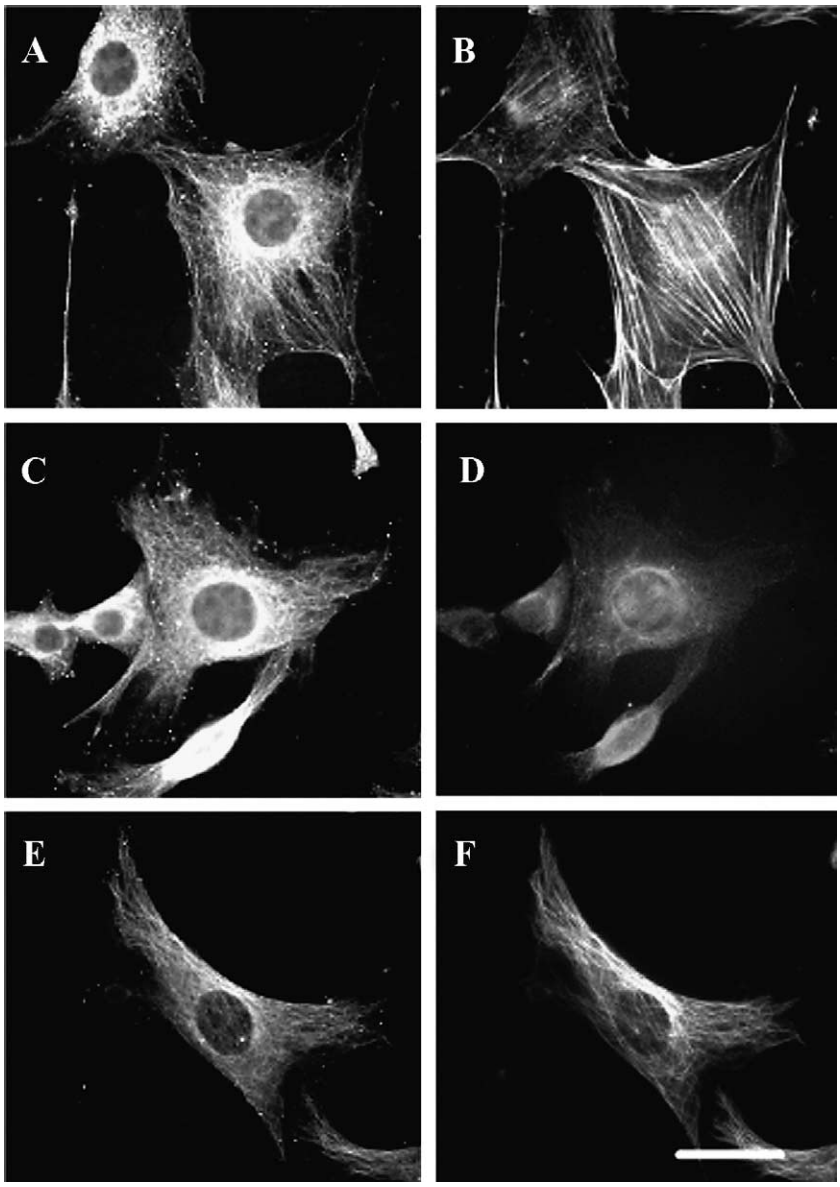

Fig. 2. Staining of NIH3T3 cells with fluorescently-tagged phalloidin, anti-desmin and anti-tubulin antibodies. Cell staining with FITC-tagged phalloidin and immunofluorescence with anti-desmin and anti-tubulin antibodies was performed as described in Section 2. (A–F) Epifluorescent micrographs. (A, B) Cells probed with TR–mOGG1 and FITC-conjugated phalloidin. (C, D) Cells probed with TR–mOGG1 and anti-desmin mouse monoclonal mAb1636 antibody followed by Alexa 488-conjugated goat anti-mouse IgG antibodies. (E, F) Cell probed with TR–mOGG1 and FITC-tagged mouse anti-tubulin antibodies. (A, C, E) TR–mOGG1 staining. (B) Phalloidin staining. (D) Immunofluorescent staining with anti-desmin antibodies. (F) Immunofluorescent staining with anti-α tubulin antibodies. (F) Bar, 25 μm applies to all panels.

proved resistant to low concentrations of non-ionic detergents (e.g., 0.5% (v/v) Triton X-100; 0.5% (v/v) Tween 20) and/or saline solutions (e.g., 600 mM NaCl) (results not shown), the specificity of this binding needed to be determined. In situ competition assays were used to assess the specificity of mOGG1 binding for tubulin assemblies. Results from these experiments are shown in Fig. 5. The decoration of a cytoplasmic microtubule network by TR–mOGG1 was suppressed when cells were probed with TR–mOGG1 in the presence of fractions enriched in mammalian tubulin (Fig. 5D). Furthermore, TR–mOGG1 decoration of tubulin assemblies such as the centriole and the mitotic spindle were also inhibited by the presence of tubulin-enriched fractions (not shown). Similar results to those shown in Fig. 5 were obtained when cells were probed with TR–hOGG1 in the presence of tubulin-enriched fractions (not shown).

3.4. Affinity binding and photo-digestion of in vitro-assembled Rose Bengal-tagged mOGG1-tubulin complexes confirm the association of mOGG1 with tubulin assemblies

To substantiate in situ binding results obtained with mOGG1, protein fractions enriched in mammalian tubulin

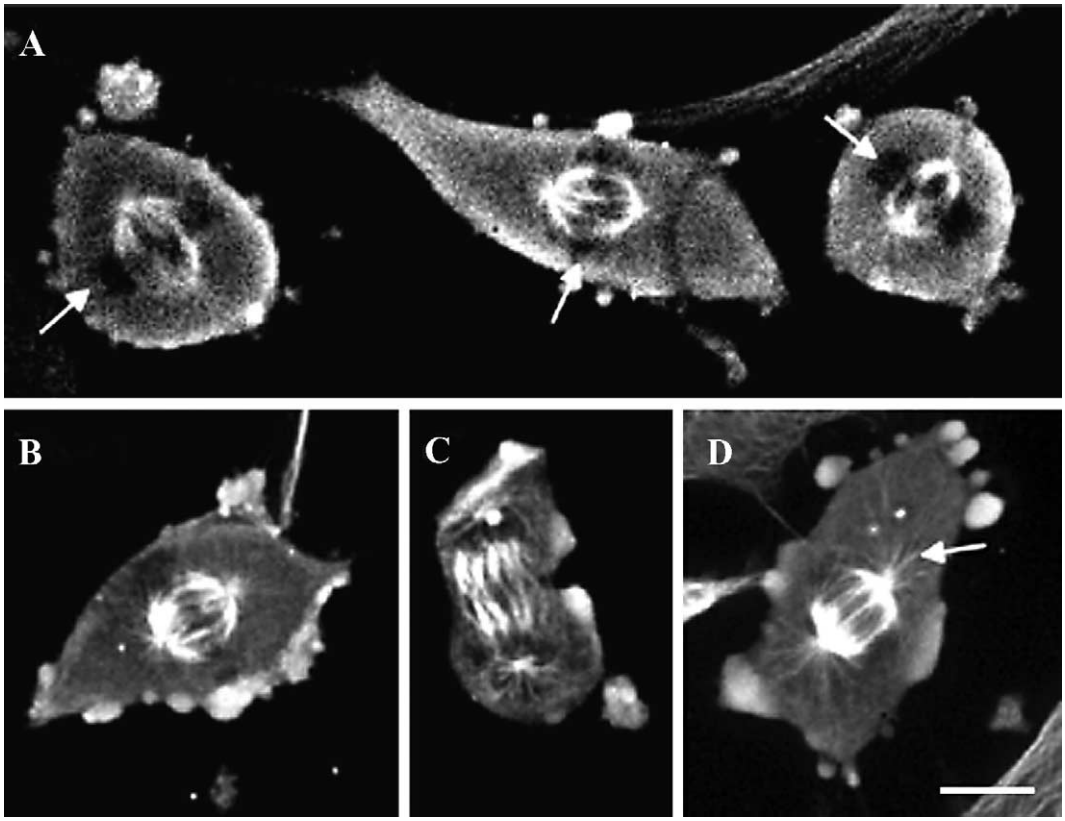

Fig. 3. Decoration of the mitotic spindle assembly by fluorescently-tagged mOGG1. Chemical conjugation of mOGG1 to Texas red and probing of mitotic cells with TR–mOGG1 was as described in Section 2. (A–D) Epifluorescent micrographs. (A–D) Cells probed with TR–mOGG1. (A) Mitotic chromosomes at the metaphase plate (arrows). (D) Astral microtubules emanating from the centrosome at the spindle pole (arrow). (A, B, D) Metaphase. (C) Anaphase. (D) Bar, 20 μm applies to all panels.

were assessed for their ability to bind mOGG1 in vitro using affinity chromatography and in vitro site-directed photocleavage analyses. Results from these experiments are shown in Fig. 6. MOGG1 affinity binding, chemical cross-linking, chemical conjugation ofmOGG1 to Rose Bengal (RB–mOGG1), in vitro site-directed photochemistry and SDS-PAGE were performed as described in Section 2. Mixtures containing fractions enriched in mammalian tubulin were incubated with either mOGG1 or BSA immobilized on to Sepharose beads. After incubation, beads were washed as for immunoprecipitation and affinity binding ligands analyzed by SDS-PAGE. SDS-PAGE analyses of affinity binding ligands revealed that only mOGG1-Sepharose beads were able to specifically retain tubulin molecules (Fig. 6A, lane 2). A small amount of mOGG1 was released from the Sepharose support during sample preparation (Fig. 6A, lane 2).

To confirm the binding specificity between mOGG1 and tubulin assemblies and circumvent problems associated with the analysis of relatively large macromolecular conjugates formed as a result of chemical cross-linking analyses, including those formed between mOGG1 and microtubules (not shown), in vitro site-directed protein photoreaction was applied to confirm the formation of mOGG1–tubulin complexes. This site-directed technique was shown previously to be an effective technique to confirm the association of ligands with specific elements of the cytoskeleton [47]. Results from these in vitro photochemical experiments are shown in Fig. 6B. Protein mixtures containing tubulin-enriched fractions and either unconjugated mOGG1 (Fig. 6B, top gel, lanes 1 and 3) or RB–mOGG1 (Fig. 6B, top gel, lanes 2 and 4) or protein mixtures containing mammalian actin and tubulin-enriched fractions and either unconjugated mOGG1 (Fig. 6B, bottom gel, lanes 1 and 3) or RB–mOGG1 (Fig. 6B, bottom gel, lanes 2 and 4) were incubated in the absence (Fig. 6B, lanes 1 and 2) or the presence (Fig. 6B, lanes 3 and 4) of visible light. After irradiation, protein samples were analyzed by SDS-PAGE and protein bands identified by Coomassie blue staining. Tubulin migrated on SDS-PAGE gels at its expected mobility either in the presence of unconjugated mOGG1 or RB–mOGG1 in the absence of visible light (Fig. 6B, lanes 1 and 2, respectively) or in the presence of unconjugated mOGG1 and visible light (Fig. 6B, lane 3). However, SDS-PAGE gels showed that tubulin was photo-digested in the presence of RB–mOGG1 and visible light (Fig. 6B, lane 4) and the actin band (a non-specific control) remained unchanged at its expected mobility (Fig. 6B, bottom gel, lane 4).

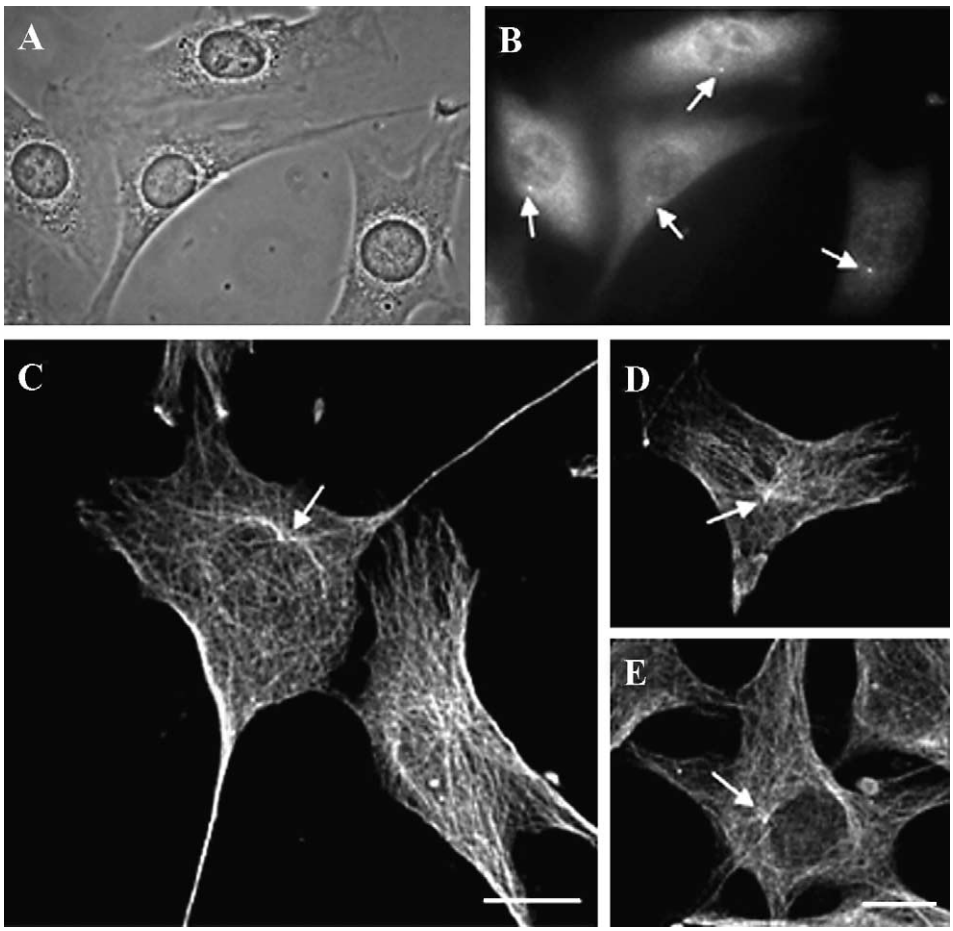

Fig. 4. Decoration of the centrosome/centriole in interphase cells by fluorescently-tagged mOGG1. Chemical conjugation of mOGG1 to Texas red and cell probing with TR–mOGG1 was as described in Fig. 1. (A) Phase contrast micrograph. (B–E) Epifluorescent micrographs. (A, B) Cells probed with anti-γ tubulin antibodies. (C–E) Cells probed with TR–mOGG1. (B–E) Centrosome/centriole (arrows). (C) Bar, 20 μm. (E) Bar 20 μm applies to panels A, B, D, E.

3.5. Cells probed with RB–mOGG1 or RB-anti-mOGG1 antibodies in the presence of visible light showed disruption of their microtubules

In situ site-directed photodigestion of proteins was also shown to be an effective method to evaluate the binding of specific ligands to elements of the cytoskeleton [45]. In situ site-directed protein photodigestion was used to evaluate the extent of microtubule disruption in RB–mOGG1-treated cells. Results from these experiments are shown in Fig. 7. Cell probing with RB–mOGG1 and in situ site-directed photochemistry was as described in Section 2. Cells probed with unmodified mOGG1 in the presence of visible light (Fig. 7A and B) did not show detectable changes in their microtubule networks. Microtubules were disrupted, however, in cells probed with RB–mOGG1 in the presence of visible light (Fig. 7C and D). Disruption of microtubules was most notable near the peripheral cytoplasm of cells exposed to RB–mOGG1 and visible light (Fig. 7C and D). Microtubules were not disrupted when these experiments were conducted in the absence of visible light (not shown). Similar results to those shown in Fig. 7 were obtained when cells were probed with Rose Bengal-conjugated anti-mOGG1 antibodies instead of RB–mOGG1 and irradiated with visible light (Fig. 8).

4. Discussion

Although studies focusing on OGG1 have been largely directed at elucidating its enzymatic activity, some have turned attention to its cellular distribution. To date, various in situ localization methods have been applied to investigate OGG1 distribution in actively growing tissue culture cells. Results from in situ localization studies have shown that OGG1 is distributed between the two major compartments of the cell, the nucleus and the cytoplasm [25–28,44]. These observations are not surprising considering the amount of DNA residing in the nucleus and the large volume of mitochondrial and protein synthesis activity that resides in the cytoplasm.

Recently, however, indirect immunofluorescent localization analyses using anti-mOGG1 antibodies revealed that cytoplasmic mOGG1 staining was not diffuse throughout but instead seemed organized along strands. This staining pattern

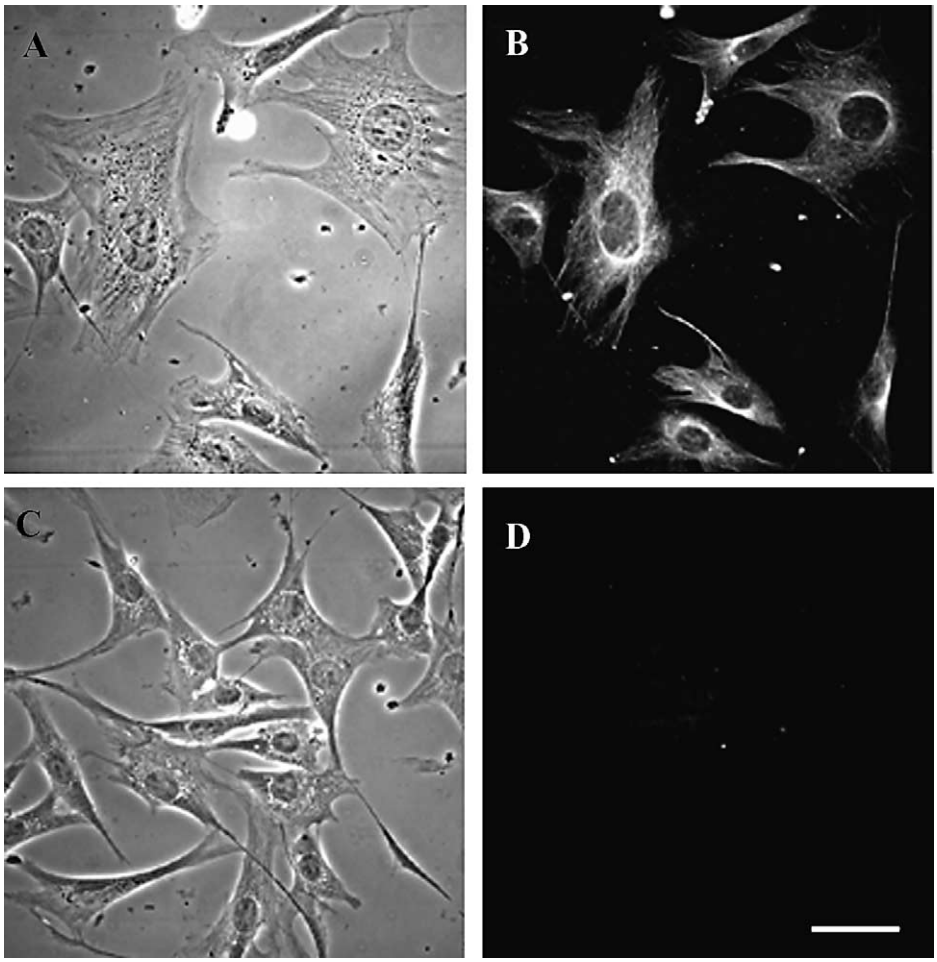

Fig. 5. Inhibition of the decoration of microtubules by fluorescently-tagged mOGG1 through tubulin-competitive binding. Chemical conjugation of mOGG1 to Texas red and cell probing with TR–mOGG1 was as described in Fig. 1. 1. (A, C) Phase contrast micrographs. (B, D) Epifluorescent micrographs. (A, B) Cells probed with TR–mOGG1 in the absence of tubulin-enriched fractions. (C, D) Cells probed with TR–mOGG1 in the presence of tubulin-enriched fractions. (D) Bar, 25 μm applies to all panels.

suggested that at least a fraction of the cytoplasmic mOGG1 pool may be associated with filament-like structures. In addition, cell exposure to oxidative DNA damage induced the redistribution of cytoplasmic mOGG1 pools to the nucleus and its peripheral cytoplasm [44]. The relatively rapid redistribution of mOGG1 under these experimental conditions suggested that a form of active transport may be involved in the relocation process.

This study used recombinant mOGG1 tagged to fluorescent and photosensitive dye molecules to directly probe actively growing tissue culture cells in an effort to detect associations between mOGG1 and cytoplasmic filaments. Results from these in situ localization studies showed that mOGG1 binds microtubules, one of the three main polymers constituting the cell cytoskeleton. Furthermore, evidence presented here revealed that mOGG1 association with the cytoskeleton was maintained throughout the cell cycle. During interphase fluorescently-tagged mOGG1 decorated an extensive network of microtubules emanating from the nuclear periphery and the centriole/centrosome. At mitosis, fluorescently-tagged mOGG1 was found associated with microtubules participating in the spindle assembly and centriole/centrosome. This last observation may be significant from the stand point of DNA repair, since it has been shown that centrosomes play a critical role in cell cycle progression as well as cellular responses to defects in DNA replication and the onset of DNA damage [42,43].

In situ localization results obtained with fluorescently-tagged mOGG1 were substantiated by results obtained combining chemical cross-linking and site-directed photodigestion analyses. The application of chemical cross-linking analyses proved of limited use in this case since the cross-linking agents used had a tendency to form conjugates not suitable for evaluation by gel shifting and immunoblot analyses. This observation was not surprising since cross-linking agents would covalently-link mOGG1 with entire microtubule segments or several of their subunits all of which would have molecular masses too large for resolving on SDS-PAGE gels. In contrast to chemical cross-linking analyses, site-directed photodigestion, a method previously

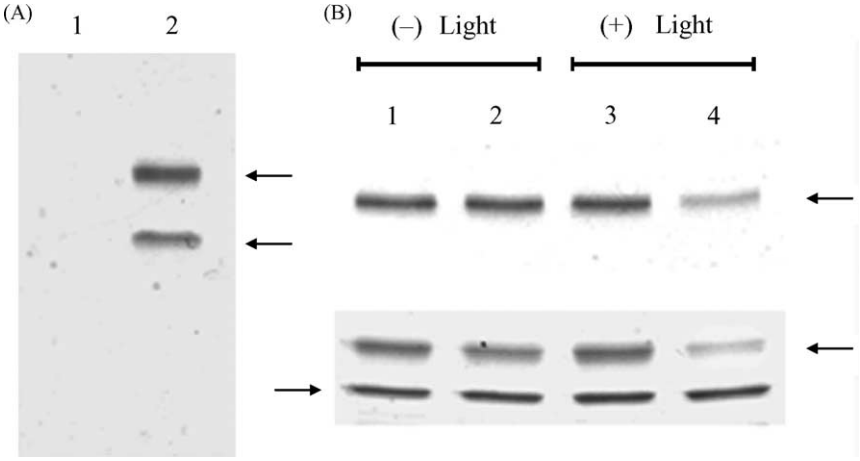

Fig. 6. Affinity binding of mOGG1–tubulin complexes and in vitro site-directed photochemical digestion of tubulin subunits from RB–mOGG1–tubulin complexes. Affinity binding to Sepharose-immobilized ligands, DMS chemical cross-linking, in vitro photochemical digestion of tubulin from RB–mOGG1–tubulin complexes and SDS-PAGE were conducted as described in Section 2. (A) Coomassie blue stained SDS-PAGE gel containing proteins bound to either Sepharose-immobilized BSA or Sepharose-immobilized mOGG1. Lane 1, tubulin-enriched fraction bound to BSA-Sepharose beads; lane 2, tubulin-enriched fraction bound to mOGG1-Sepharose beads. (B) Tubulin-enriched fractions were reacted either in the absence (top gel) or in the presence (bottom gel) of actin with either unconjugated mOGG1 or RB–mOGG1 in the absence (lanes 1 and 2) or the presence (lanes 3 and 4) of visible light and photo-digestion reactions analyzed by SDS-PAGE. (Top gel) Each lane of a 7.5–15% (w/v) SDS-polyacrylamide gel was loaded with reaction mixtures containing 5 μg of tubulin and 320 ng of either unconjugated mOGG1 or RB–mOGG1. (Bottom gel) Each lane of a 7.5–15% (w/v) SDS-polyacrylamide gel was loaded with reaction mixtures containing 5 μg of tubulin, 4 μg actin and 320 ng of either unconjugated mOGG1 or RB–mOGG1. Reaction mixtures were irradiated for 60 min at 37 °C. Gels were stained overnight with Coomassie blue. Lanes 1 and 3 show the tubulin band in reaction mixtures containing unconjugated mOGG1. Lanes 2 and 4 show the tubulin band in reaction mixtures containing RB–mOGG1. (A) Arrows at right indicate the migration positions of tubulin (top) and mOGG1 (bottom). (B) Arrow to the left points to the migration position of actin. Arrows to the right point to the migration position of tubulin.

used to analyze cytoskeletal elements and their ligands, proved ideal for this purpose. In situ and in vitro site-directed photoreactions showed the digestion of tubulin subunits from mOGG1–microtubule complexes, thus, confirming the association of mOGG1 with microtubules and their tubulin subunits. Furthermore, cells probed with RB-anti-mOGG1 antibodies showed disruption of their microtubule networks upon irradiation (Fig. 8), indicating that a fraction of intrinsic (authentic) mOGG1 is associated with microtubules. The relatively strong affinity shown by mOGG1 for tubulin molecules and their polymeric structures was not unique to the murine OGG1 nor was it conferred by its chemical conjugation to dye molecules since unconjugated mOGG1 and its human counterpart (hOGG1) were also capable of decorating microtubules in situ and site-directing the photodigestion of tubulin in vitro.

If cytoplasmic OGG1 pools associate with microtubules as shown in this report, this phenomenon would explain the filamentous-like staining pattern observed previously using indirect immunofluorescence and anti-mOGG1 antibodies. Thus, anti-mOGG1 antibodies recognized mOGG1 fractions that were bound to microtubules as well as mOGG1 localized elsewhere in the cytoplasm. On the other hand, when using fluorescently-tagged mOGG1 or hOGG1 to directly probe cells, these fluorescent probes decorated microtubules by either displacing the fraction of cellular mOGG1 bound to microtubules through competitive binding and/or fluorescently-tagged OGG1 recognized unoccupied binding sites on microtubules. The net result from either one of these possibilities would be a signal amplification well above that obtained with indirect immunofluorescence alone. This may be the case, since cells probed with untagged mOGG1 and then treated for indirect immunofluorescence with anti-mOGG1 antibodies gave similar fluorescent images to those obtained from cells probed directly with fluorescently-tagged mOGG1 (not shown). Taken together these observations suggest that this equilibrium persists through the cell cycle keeping a steady-state fraction of the cytoplasmic OGG1 pool associated with microtubules. Currently, we are conducting experiments to test the possibility that this equilibrium may shift when cells go through mitosis or are exposed to oxidative DNA damage. Results from this experimental work is beyond the scope of this report and will be reported elsewhere.

Interestingly, in our previous experiments we had also observed the filamentous staining pattern with antibodies directed against 8-oxoG. We do not expect this staining to result from 8-oxoG associated with microtubule-binding OGG1, since the affinity of 8-oxoG mononucleotides to this enzyme is low (D.O.Z., unpublished). Rather, a plausible explanation for this phenomenon would be provided by binding of 8-oxoGTP in the nucleotide-binding center of tubulin, which is regulated by GTP. The cellular pool of GTP and dGTP is prone to oxidation, and a special enzyme, MutT (MTH in eukaryotes), hydrolyzes both ribo- and deoxyriboguanosine triphosphates oxidized at C8 [55]. However, eukaryotic MTH is mostly localized to the cell compartment supporting DNA

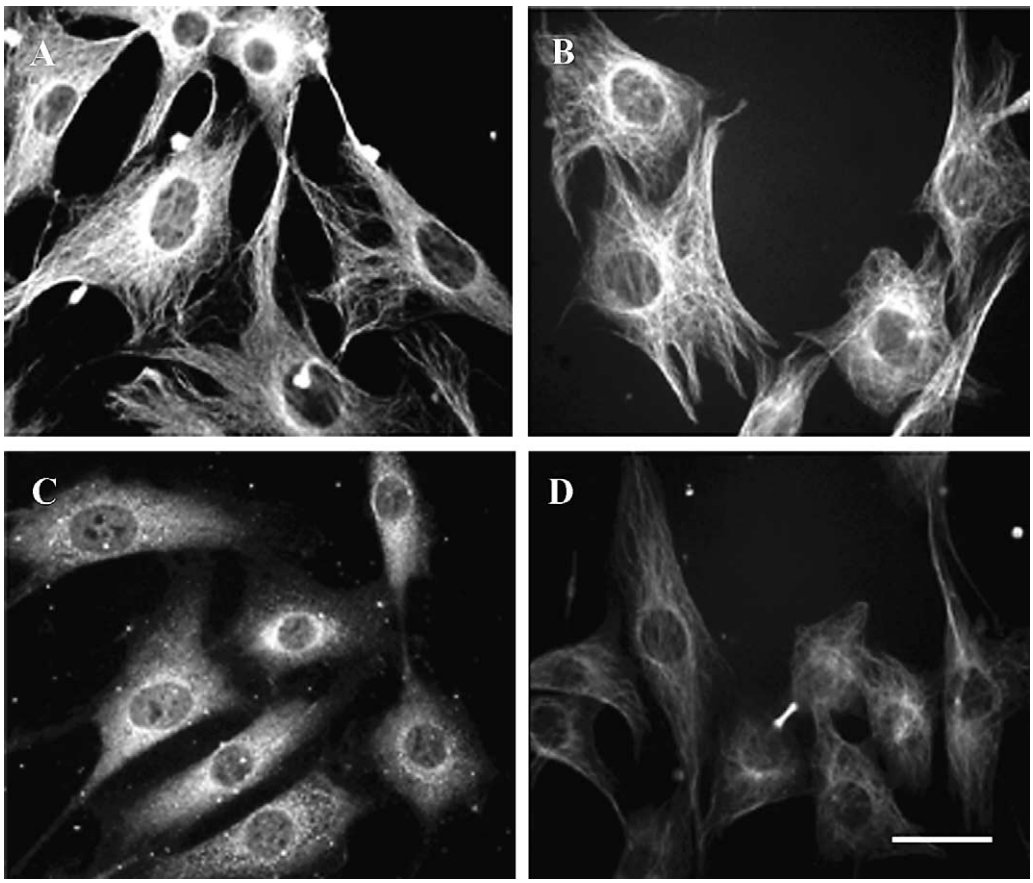

Fig. 7. In situ site-directed disruption of microtubules by Rose Bengal-conjugated mOGG1. NIH3T3 fibroblasts were grown on slides, fixed with paraformaldehyde, washed with MSM-Pipes and incubated with RB–mOGG1 or unconjugated mOGG1. Cells were irradiated for 60 min at 37 °C. (A–D) Epifluorescent micrographs. (A, B) Cells irradiated in the presence of unconjugated mOGG1. (C, D) Cells irradiated in the presence of RB–mOGG1. (A, C) Microtubules decorated with 16 μg/ml Alexa 568-conjugated mOGG1. (B, D) Microtubules decorated with FITC-tagged mouse anti-α tubulin antibodies. (D) Bar, 25 μm applies to all panels.

replication, such as the nucleus and mitochondria [29], and therefore, cytoplasmic pools of 8-oxoGTP could be significantly higher than the nuclear or mitochondrial pool, possibly allowing part of 8-oxoGTP to be associated with tubulin.

To our knowledge the observation that mOGG1 associates with microtubules, a widely distributed cytoskeletal component, has not been reported previously. Failure to observe this binding phenomenon may be explained as follows: either the in situ localization techniques used were detrimental to the integrity of microtubules and/or cell expression of GFP-tagged probes or GFP-OGG1 constructs themselves may have a lower affinity for or not bind microtubules in vivo. As suggested earlier, the OGG1 fraction bound to microtubules may be relatively small by comparison to the OGG1 pool found elsewhere in the cytoplasm, thus, making it difficult to detect by immunofluorescence. Furthermore, microtubule ends grow leading to elongation or their tubulin subunits depolymerize leading to shortening in response to cellular demands; experimentally, however, they are particularly susceptible to catastrophic shortening (e.g., cold, hydrostatic pressure, etc.). Any one of the above scenarios would preclude previous studies from detecting the formation of OGG1-microtubule complexes in situ.

Although the association of mOGG1 with microtubules can not be ruled out as an artifact, this scenario seems unlikely since the murine and human OGG1 isoforms showed this same property. Light-induced disruption of microtubules by RB-conjugated anti-mOGG1 antibodies proves that microtubules are not only potential sites of binding for externally applied mOGG1, but the intrinsic OGG1 protein is also associated with these cytoskeletal elements. There is already evidence that OGG1 may have the ability to associate with structural components of the cell. Dantzer and collaborators, using a stable transfectant cell line expressing hOGG1 fused to GFP, showed that hOGG1 was preferentially associated with the nuclear matrix at interphase [31]; the nuclear matrix is largely composed of filamentous proteins (e.g., the lamins), many of which, play roles similar to that of components of the cytoskeleton. Because of these similarities, the nuclear matrix is often referred to as the karyoskeleton [56,57]. Association of hOGG1 with the karyoskeleton was directed by serine phosphorylation of the protein [31]; it is possible that

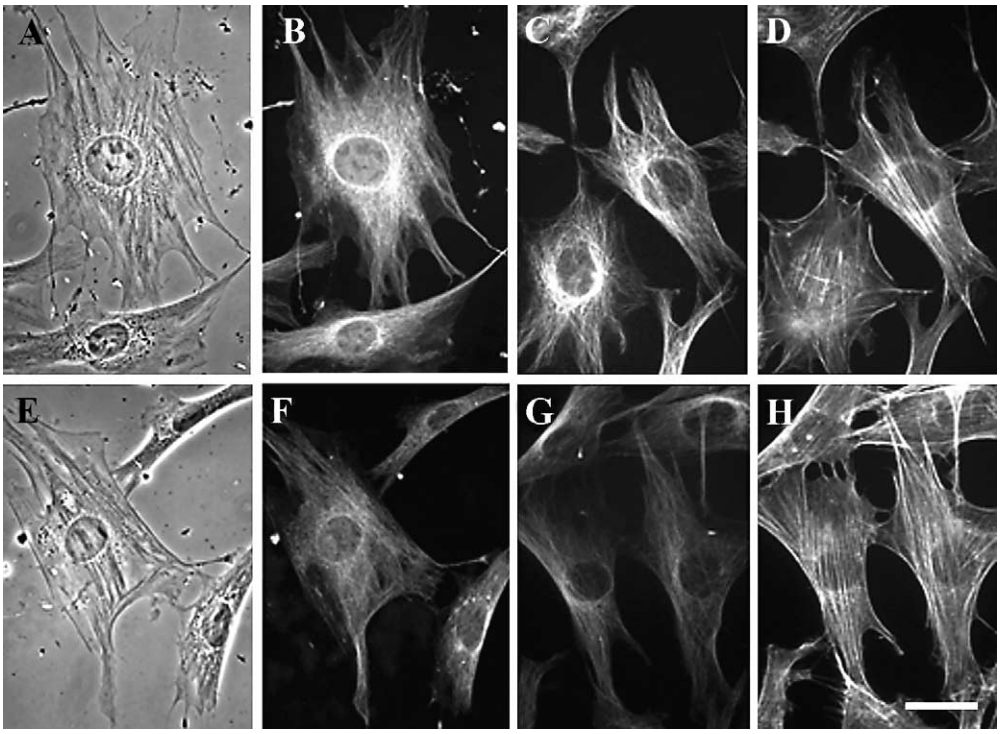

Fig. 8. In situ site-directed disruption of microtubules by Rose Bengal-conjugated anti-mOGG1 antibodies. NIH3T3 fibroblasts were grown on slides, treated as in Fig. 7 and incubated with RB-conjugated anti-mOGG1 antibodies or unconjugated anti-mOGG1 antibodies. Cells were irradiated for 60 min at 37 °C. (A, E) Phase contrast micrographs. (B–D, F–H) Epifluorescent micrographs. (A–D) Cells irradiated in the presence of unconjugated anti-mOGG1 antibodies. (E–H) Cells irradiated in the presence of RB-conjugated anti-mOGG1 antibodies. (A, B, E, F) Microtubules decorated with 16 μg/ml Alexa 568-conjugated mOGG1. (C, G) Microtubules decorated with FITC-tagged mouse anti-α tubulin antibodies. (D, H) F-actin decorated with FITC-conjugated phalloidin. (H) Bar, 25 μm applies to all panels.

this phosphorylation regulates the distribution of OGG1 between nuclear and cytoplasmic cytoskeleton networks.

Actin filaments, intermediate filaments and microtubules interact with each other and with associated proteins to form the cytoskelton and mediate cellular trafficking [32–36]. Cytoskeletal trafficking efficiently mobilizes a wide range of macromolecules and small organelles. For example, microtubules, the largest and most rigid of the three major cytoskeletal filaments, in conjunction with microtubule-associated proteins (MAPs) and molecular motor proteins, provide paths along which macromolecules are transported to or from the nuclear compartment or within the cytoplasmic compartment [39,40]. By playing an important role in intracellular transport, microtubules assist cells with the deployment of essential resources to defined sites, thus, maximizing their utilization. Transport along microtubules also provides an extremely fast mechanism to regulate protein activity, particularly for proteins whose main function is primarily restricted to a cell compartment (e.g., the nucleus). An example of such a protein is the tumor-suppressor protein p53. P53 rides on microtubules while shuttling to the nucleus in response to stress, and its activity is modulated in taxol-treated cells [58–60].

The observation that tubulin-enriched fractions inhibited fluorescently-tagged mOGG1 from decorating microtubules by competitive binding does not rule out the possibility that mOGG1 interaction with microtubules may be transient or mediated through intermediate(s) yet to be identified. Furthermore, modifications introduced by chemical conjugation to dye molecules did not alter mOGG1's capacity to bind microtubules. Also, the addition of an hexahistidine tag to the *N*-terminus of hOGG1 through a thirteen amino acid-long linker did not preclude hOGG1 constructs from binding microtubules, implying that its *N*-terminus may not be directly involved in the binding process. Taken together these observations suggest that OGG1's capacity to associate with tubulin molecules may not be easily perturbed.

Hypotheses suggesting that MAPs or motor proteins may be forming a bridge between mOGG1 and tubulin subunits is an attractive model in light of the results presented here. This type of intracellular transport has already been shown to occur for other small macromolecules (proteins and nucleic acids), thus, it is possible that OGG1 and other DNA repair enzymes are using motor proteins riding on microtubules as a mechanism to regulate their activity while relocating in the cytoplasm and shuttling to the nucleus. On the other hand, microtubule-disrupting drugs are among the most effective anti-cancer chemotherapeutic agents and conceivably their effectiveness may be in part derived from their capacity to disrupt intracellular transport in general and of DNA re-

pair enzymes in particular; for instance, taxol, a microtubule-selective agent, is known to markedly slow down the repair of many kinds of DNA damage [61]. The end result would be an increase in DNA damage and cell death. Studies are currently underway in our laboratory to test these and related hypotheses.

Acknowledgment

We wish to thank Wen Hui Feng, Rebecca Rowehl, LeeAnn Silver, and Gregory Rudomen for expert technical assistance. This work was supported by research grants CA8403301 from the National Cancer Institute (to M.B.), 02-04-49605 from the Russian Foundation for Basic Research and PD02-1.4-469 from the Russian Ministry of Education (to D.O.Z.).

References

[1] Y. Tsurudome, T. Hirano, H. Yamato, I. Tanaka, M. Sagai, H. Hirano, N. Nagata, H. Itoh, H. Kasai, Changes in levels of 8-hydroxyguanine in DNA, its repair and OGG1 mRNA in rat lungs after intratracheal administration of diesel exhaust particles, Carcinogenesis 20 (1999) 1573–1576.

[2] H.N. Kim, Y. Morimoto, T. Tsuda, Y. Ootsuyama, M. Hirohashi, T. Hirano, I. Tanaka, Y. Lim, I.G. Yun, H. Kasai, Changes in DNA 8-hydroxyguanine levels, 8-hydroxyguanine repair activity, and hOGG1 and hMTH1 mRNA expression in human lung alveolar epithelial cells induced by crocidolite asbestos, Carcinogenesis 22 (2001) 265–269.

[3] A. Kinoshita, H. Wanibuchi, S. Imaoka, M. Ogawa, C. Masuda, K. Morimura, Y. Funae, S. Fukushima, Formation of 8-hydroxydeoxyguanosine and cell-cycle arrest in the rat liver via generation of oxidative stress by phenobarbital: association with expression profiles of p21(WAF1/Cip1), cyclin D1 and Ogg1, Carcinogenesis 23 (2002) 341–349.

[4] K.A. Conlon, A.P. Grollman, M. Berrios, Immunolocalization of 8-oxoguanine in nutrient-deprived mammalian tissue culture cells, J. Histotech. 23 (2000) 37–44.

[5] H. Kasai, H. Tanooka, S. Nishimura, Formation of 8-hydroxyguanine residues in DNA by X-irradiation, Gann 75 (1984) 1037–1039.

[6] H. Kasai, P.F. Crain, Y. Kuchino, S. Nishimura, A. Ootsuyama, H. Tanooka, Formation of 8-hydroxyguanine moiety in cellular DNA by agents producing oxygen radicals and evidence for its repair, Carcinogenesis 7 (1986) 1849–1851.

[7] J.L. Ravanat, J. Cadet, Reaction of singlet oxygen with 2′-deoxyguanosine and DNA. Isolation and characterization of the main oxidation products, Chem. Res. Toxicol. 8 (1995) 379–388.

[8] K. Tsuruya, M. Furuichi, Y. Tominaga, M. Shinozaki, M. Tokumoto, T. Yoshimitsu, K. Fukuda, H. Kanai, H. Hirakata, M. Iida, Y. Nakabeppu, Accumulation of 8-oxoguanine in the cellular DNA and the alteration of the OGG1 expression during ischemia-reperfusion injury in the rat kidney, DNA Repair (Amst.) 2 (2003) 211–229.

[9] D.C. Malins, R. Haimanot, Major alterations in the nucleotide structure of DNA in cancer of the female breast, Cancer Res. 51 (1991) 5430–5432.

[10] D.C. Malins, Identification of hydroxyl radical-induced lesions in DNA base structure: biomarkers with a putative link to cancer development, J. Toxicol. Environ. Health 40 (1993) 247–261.

[11] J.P. Spencer, A. Jenner, O.I. Aruoma, P.J. Evans, H. Kaur, D.T. Dexter, P. Jenner, A.J. Lees, D.C. Marsden, B. Halliwell, Intense oxidative DNA damage promoted by L-dopa and its metabolites. Implications for neurodegenerative disease, FEBS Lett. 353 (1994) 246–250.

[12] Z.I. Alam, A. Jenner, S.E. Daniel, A.J. Lees, N. Cairns, C.D. Marsden, P. Jenner, B. Halliwell, Oxidative DNA damage in the parkinsonian brain: an apparent selective increase in 8-hydroxyguanine levels in substantia nigra, J. Neurochem. 69 (1997) 1196–1203.

[13] P. Degan, M.K. Shigenaga, E.M. Park, P.E. Alperin, B.N. Ames, Immunoaffinity isolation of urinary 8-hydroxy-2′-deoxyguanosine and 8-hydroxyguanine and quantitation of 8-hydroxy-2′-deoxyguanosine in DNA by polyclonal antibodies, Carcinogenesis 12 (1991) 865–871.

[14] H. Kasai, S. Nishimura, DNA damage induced by asbestos in the presence of hydrogen peroxide, Gann 75 (1984) 841–844.

[15] A.P. Grollman, M. Moriya, Mutagenesis by 8-oxoguanine: an enemy within, Trends Genet. 9 (1993) 246–249.

[16] J.L. Ravanat, R.J. Turesky, E. Gremaud, L.J. Trudel, R.H. Stadler, Determination of 8-oxoguanine in DNA by gas chromatography–mass spectrometry and HPLC—electrochemical detection: overestimation of the background level of the oxidized base by the gas chromatography–mass spectrometry assay, Chem. Res. Toxicol. 8 (1995) 1039–1045.

[17] F. Yamamoto, H. Kasai, T. Bessho, M.H. Chung, H. Inoue, E. Ohtsuka, T. Hori, S. Nishimura, Ubiquitous presence in mammalian cells of enzymatic activity specifically cleaving 8-hydroxyguanine-containing DNA, Jpn. J. Cancer Res. 83 (1992) 351–357.

[18] T.A. Rosenquist, D.O. Zharkov, A.P. Grollman, Cloning and characterization of a mammalian 8-oxoguanine DNA glycosylase, Proc. Natl. Acad. Sci. U.S.A. 94 (1997) 7429–7434.

[19] M.H. Chung, H.S. Kim, E. Ohtsuka, H. Kasai, F. Yamamoto, S. Nishimura, An endonuclease activity in human polymorphonuclear neutrophils that removes 8-hydroxyguanine residues from DNA+, Biochem. Biophys. Res. Commun. 178 (1991) 1472–1478.

[20] T. Bessho, K. Tano, H. Kasai, E. Ohtsuka, S. Nishimura, Evidence for two DNA repair enzymes for 8-hydroxyguanine (7,8-dihydro-8-oxoguanine) in human cells, J. Biol. Chem. 268 (1993) 19416–19421.

[21] M. Tani, K. Shinmura, T. Kohno, T. Shiroishi, S. Wakana, S.R. Kim, T. Nohmi, H. Kasai, S. Takenoshita, Y. Nagamachi, J. Yokota, Genomic structure and chromosomal localization of the mouse *Ogg1* gene that is involved in the repair of 8-hydroxyguanine in DNA damage, Mamm. Genome 9 (1998) 32–37.

[22] R. Lu, H.M. Nash, G.L. Verdine, A mammalian DNA repair enzyme that excises oxidatively damaged guanines maps to a locus frequently lost in lung cancer, Curr. Biol. 7 (1997) 397–407.

[23] A. Klungland, I. Rosewell, S. Hollenbach, E. Larsen, G. Daly, B. Epe, E. Seeberg, T. Lindahl, D.E. Barnes, Accumulation of premutagenic DNA lesions in mice defective in removal of oxidative base damage, Proc. Natl. Acad. Sci. U.S.A. 96 (1999) 13300– 13305.

[24] O. Minowa, T. Arai, M. Hirano, Y. Monden, S. Nakai, M. Fukuda, M. Itoh, H. Takano, Y. Hippou, H. Aburatani, K. Masumura, T. Nohmi, S. Nishimura, T. Noda, *Mmh*/*Ogg1* gene inactivation results in accumulation of 8-hydroxyguanine in mice, Proc. Natl. Acad. Sci. U.S.A. 97 (2000) 4156–4161.

[25] H. Aburatani, Y. Hippo, T. Ishida, R. Takashima, C. Matsuba, T. Kodama, M. Takao, A. Yasui, K. Yamamoto, M. Asano, Cloning and characterization of mammalian 8-hydroxyguanine-specific DNA glycosylase/apurinic, apyrimidinic lyase, a functional mutM homologue, Cancer Res. 57 (1997) 2151–2156.

[26] M. Takao, H. Aburatani, K. Kobayashi, A. Yasui, Mitochondrial targeting of human DNA glycosylases for repair of oxidative DNA damage, Nucleic Acids Res. 26 (1998) 2917–2922.

[27] K. Nishioka, T. Ohtsubo, H. Oda, T. Fujiwara, D. Kang, K. Sugimachi, Y. Nakabeppu, Expression and differential intracellular localization of two major forms of human 8-oxoguanine DNA glycosylase encoded by alternatively spliced OGG1 mRNAs, Mol. Biol. Cell. 10 (1999) 1637–1652.

[28] K. Shinmura, T. Kohno, M. Takeuchi-Sasaki, M. Maeda, T. Segawa, T. Kamo, H. Sugimura, J. Yokota, Expression of the OGG1-type 1a (nuclear form) protein in cancerous and non-cancerous human cells, Int. J. Oncol. 16 (2000) 701–707.
[29] Y. Nakabeppu, Regulation of intracellular localization of human MTH1, OGG1, and MYH proteins for repair of oxidative DNA damage, Prog. Nucleic Acid Res. Mol. Biol. 68 (2001) 75–94.
[30] I. Boldogh, D. Milligan, M.S. Lee, H. Bassett, R.S. Lloyd, A.K. McCullough, hMYH cell cycle-dependent expression, subcellular localization and association with replication foci: evidence suggesting replication-coupled repair of adenine:8-oxoguanine mispairs, Nucleic Acids Res. 29 (2001) 2802–2809.
[31] F. Dantzer, L. Luna, M. Bjoras, E. Seeberg, Human OGG1 undergoes serine phosphorylation and associates with the nuclear matrix and mitotic chromatin in vivo, Nucleic Acids Res. 30 (2002) 2349–2357.
[32] T.D. Pollard, J.A. Cooper, Actin and actin-binding proteins. A critical evaluation of mechanisms and functions, Annu. Rev. Biochem. 55 (1986) 987–1035.
[33] M. Schliwa, The Cytoskeleton: An Introductory Survey, Springer-Verlag, New York, 1986.
[34] S.L. Rogers, I.S. Tint, P.C. Fanapour, V.I. Gelfand, Regulated bidirectional motility of melanophore pigment granules along microtubules in vitro, Proc. Natl. Acad. Sci. U.S.A. 94 (1997) 3720–3725.
[35] A. Blocker, F.F. Severin, J.K. Burkhardt, J.B. Bingham, H. Yu, J.C. Olivo, T.A. Schroer, A.A. Hyman, G. Griffiths, Molecular requirements for bi-directional movement of phagosomes along microtubules, J. Cell. Biol. 137 (1997) 113–129.
[36] J.D. Huang, S.T. Brady, B.W. Richards, D. Stenolen, J.H. Resau, N.G. Copeland, N.A. Jenkins, Direct interaction of microtubule- and actin-based transport motors, Nature 397 (1999) 267–270.
[37] G. Bassell, R.H. Singer, Singer, mRNA and cytoskeletal filaments, Curr. Opin. Cell Biol. 9 (1997) 109–115.
[38] J.S. Pachter, Association of mRNA with the cytoskeletal framework: its role in the regulation of gene expression, Crit. Rev. Eukaryot. Gene Expr. 2 (1992) 1–18.
[39] R.D. Allen, D.G. Weiss, J.H. Hayden, D.T. Brown, H. Fujiwake, M. Simpson, Gliding movement of and bidirectional transport along single native microtubules from squid axoplasm: evidence for an active role of microtubules in cytoplasmic transport, J. Cell. Biol. 100 (1985) 1736–1752.
[40] V. Prahlad, B.T. Helfand, G.M. Langford, R.D. Vale, R.D. Goldman, Fast transport of neurofilament protein along microtubules in squid axoplasm, J. Cell Sci. 113 (Pt. 22) (2000) 3939–3946.
[41] C.L. Rieder, S. Faruki, A. Khodjakov, The centrosome in vertebrates: more than a microtubule-organizing center, Trends Cell Biol. 11 (2001) 413–419.
[42] O.C. Sibon, A. Kelkar, W. Lemstra, W.E. Theurkauf, DNA-replication/DNA-damage-dependent centrosome inactivation in *Drosophila* embryos, Nat. Cell Biol. 2 (2000) 90–95.
[43] H.M. Hut, W. Lemstra, E.H. Blaauw, G.W. Van Cappellen, H.H. Kampinga, O.C. Sibon, Centrosomes split in the presence of impaired DNA integrity during mitosis, Mol. Biol. Cell. 14 (2003) 1993–2004.
[44] K.A. Conlon, D.O. Zharkov, M. Berrios, Immunofluorescent localization of the murine 8-oxoguanine DNA glycosylase (mOGG1) in cells growing under normal and nutrient deprivation conditions, DNA Repair (Amst.) 2 (2003) 1337–1352.
[45] K.A. Conlon, T. Rosenquist, M. Berrios, Site-directed photochemical disruption of the actin cytoskeleton by actin-binding Rose Bengal-conjugates, J. Photochem. Photobiol. B 68 (2002) 140–146.
[46] M. Berrios, P.A. Fisher, A myosin heavy-chain-like polypeptide is associated with the nuclear envelope in higher eukaryotic cells, J. Cell. Biol. 103 (1986) 711–724.
[47] K.A. Conlon, M. Berrios, Light-induced proteolysis of myosin heavy chain by Rose Bengal-conjugated antibody complexes, J. Photochem. Photobiol. B 65 (2001) 22–28.
[48] G. Crevel, H. Huikeshoven, S. Cotterill, M. Simon, J. Wall, A. Philpott, R.A. Laskey, M. McConnell, P.A. Fisher, M. Berrios, Molecular and cellular characterization of CRP1, a *Drosophila* chromatin decondensation protein, J. Struct. Biol. 118 (1997) 9–22.
[49] P.A. Fisher, M. Berrios, G. Blobel, Isolation and characterization of a proteinaceous subnuclear fraction composed of nuclear matrix peripheral lamina and nuclear pore complexes from embryos of *Drosophila melanogaster*, J. Cell. Biol. 92 (1982) 674–686.
[50] D.E. Smith, Y. Gruenbaum, M. Berrios, P.A. Fisher, Biosynthesis and interconversion of *Drosophila* nuclear lamin isoforms during normal growth and in response to heat shock, J. Cell. Biol. 105 (1987) 771–790.
[51] R. Millonig, H. Salvo, U. Aebi, Probing actin polymerization by intermolecular cross-linking, J. Cell. Biol. 106 (1988) 785–796.
[52] M.O. Steinmetz, D. Stoffler, S.A. Muller, W. Jahn, B. Wolpensinger, K.N. Goldie, A. Engel, H. Faulstich, U. Aebi, Evaluating atomic models of F-actin with an undecagold-tagged phalloidin derivative, J. Mol. Biol. 276 (1998) 1–6.
[53] R.M. Evans, The intermediate-filament proteins vimentin and desmin are phosphorylated in specific domains, Eur. J. Cell Biol. 46 (1988) 152–160.
[54] T. Heimburg, J. Schuenemann, K. Weber, N. Geisler, Specific recognition of coiled coils by infrared spectroscopy: analysis of the three structural domains of type III intermediate filament proteins, Biochemistry 35 (1996) 1375–1382.
[55] F. Taddei, H. Hayakawa, M. Bouton, A. Cirinesi, I. Matic, M. Sekiguchi, M. Radman, Counteraction by MutT protein of transcriptional errors caused by oxidative damage, Science 278 (1997) 128–130.
[56] R. Benavente, G. Krohne, Change of karyoskeleton during spermatogenesis of *Xenopus*: expression of lamin LIV, a nuclear lamina protein specific for the male germ line, Proc. Natl. Acad. Sci. U.S.A. 82 (1985) 6176–6180.
[57] M. Berrios, N. Osheroff, P.A. Fisher, In situ localization of DNA topoisomerase II, a major polypeptide component of the *Drosophila* nuclear matrix fraction, Proc. Natl. Acad. Sci. U.S.A. 82 (1985) 4142–4146.
[58] K.H. Vousden, G.F. Woude, The ins and outs of p53, Nat. Cell Biol. 2 (2000) E178–E180.
[59] P. Giannakakou, D.L. Sackett, Y. Ward, K.R. Webster, M.V. Blagosklonny, T. Fojo, p53 is associated with cellular microtubules and is transported to the nucleus by dynein, Nat. Cell Biol. 2 (2000) 709–717.
[60] P. Giannakakou, G. Poy, Z. Zhan, T. Knutsen, M.V. Blagosklonny, T. Fojo, Paclitaxel selects for mutant or pseudo-null p53 in drug resistance associated with tubulin mutations in human cancer, Oncogene 19 (2000) 3078–3085.
[61] E. Reed, E.C. Kohn, G. Sarosy, M. Dabholkar, P. Davis, J. Jacob, M. Maher, Paclitaxel, cisplatin, and cyclophosphamide in human ovarian cancer: molecular rationale and early clinical results, Semin. Oncol. 22 (1995) 90–96.